

# DESIGN GUIDELINES FOR LOW PRESSURE AXIAL FANS BASED ON CFD-TRAINED META-MODELS

*K. Bamberger - T. Carolus*

University of Siegen  
Institute for Fluid- and Thermodynamics  
57068 Siegen, Germany  
konrad.bamberger@uni-siegen.de

## ABSTRACT

A new design strategy for low pressure axial fans is suggested. It is based on guidelines for the optimal choice of 26 geometrical parameters. Here, "optimal" means exact fulfillment of a targeted design point ( $\phi$  and  $\psi_{ts}$ ) at highest possible total-to-static efficiency. The 26 geometrical parameters describe the fan unambiguously. Hence, the suggested design process is extremely quick and simply consists of reading the optimal parameters and building up the fan geometry accordingly. The relation between targeted design point and optimal geometrical parameter is described by two-dimensional second degree polynomials. The coefficients of the polynomials are optimized by an evolutionary algorithm in which the target function is evaluated by CFD-trained meta-models. The quality of the design guidelines is then assessed by designing 81 fans according to the guidelines and conducting a CFD simulation for each design. The targeted design points of these fans are between  $0.08 \leq \phi \leq 0.24$  and  $0.06 \leq \psi_{ts} \leq 0.38$ . Good agreement between the targeted design points and the CFD results is observed. Moreover, it is shown that the total-to-static efficiencies are very high.

## NOMENCLATURE

### Latin symbols

$D$  diameter (of fan)  
 $P$  power  
 $S$  tip clearance  
 $\dot{V}$  volume flow rate

$c$  chord length  
 $d$  (max.) thickness of NACA airfoil  
 $f$  (max.) camber of NACA airfoil  
 $n$  rotational speed of fan  
 $p$  pressure  
 $r$  radius  
 $w$  relative flow velocity  
 $x$  coordinates along airfoil  
 $z$  Cartesian coordinate  
here: axis of rotation

### Greek symbols

$\alpha$  angle of attack  
 $\beta$  flow angle  
 $\gamma$  blade stagger angle  
 $\phi$  flow coefficient  
 $\eta$  efficiency

$\lambda$  sweep angle  
 $\nu$  hub-to-tip ratio  
 $\rho$  density  
 $\theta$  angle of rotation  
 $\psi$  pressure coefficient

### Abbreviations

ANN artificial neural network  
CFD computational fluid dynamics  
LE leading edge  
MLP multilayer perceptron  
RANS Reynolds-averaged Navier-Stokes  
SST shear stress transport  
TE trailing edge

### Subscripts and Indices

$I, 2$  plane up-/downstream of the fan  
 $est$  estimated  
 $h$  hub  
 $m$  midspan or meridional  
 $r$  radial  
 $t$  total or tip  
 $ts$  total-to-static  
 $tt$  total-to-total

## INTRODUCTION

This work is motivated by the need for high total-to-static efficiency of low pressure axial fans (Figure 1 shows typical examples of those machines). In many applications the total-to-static pressure rise is the design target, i.e. the dynamic pressure at the outlet of the machine is regarded as a loss since it dissipates in the surrounding atmosphere. Typically for low pressure axial fans with their large volume flow rate and moderate static pressure rise this exit loss is in the same order of magnitude as the total-to-static pressure rise. Designers of those machines face a dilemma: Either the through-flow area is as large as possible by choosing a very small hub-to-tip ratio. Consequences are a comparably small exit loss but substantial secondary flows in the hub and adjacent blade region causing excessive friction losses. On the other hand a well designed blade channel may result in a small through flow area with substantial exit losses. Objective of this study is a new design strategy which yields fans with maximum total-to-static efficiency and, at the same time, is fast and computationally inexpensive to be applied.



**Figure 1: Examples of state-of-the-art low pressure axial fans (by courtesy of Luwa, Switzerland; Helios and Voith Turbo, Germany)**

In the following, an overview of established design strategies will be given. Specific weaknesses are pointed out to emphasize the need for research on new methods. A classic design strategy is the blade element momentum method (BEM), e.g. summarized by Carolus [1]. Here the fan blade is considered as a number of stacked airfoil elements with assumed two-dimensional flow at each element. The main potential for efficiency improvements consists in the selection of optimal airfoil sections. However, the validity of this approach is strictly limited by the simplifying assumption of two-dimensional flow. An alternative approach of an inverse design method was suggested by Zangeneh in 1991 [2]. In this methodology, the blade shape is adjusted to fulfill a specific load distribution in both spanwise and streamwise direction. The flow around the blade is considered three-dimensional representing a major advantage as compared to the BEM method. However, there are still simplifying assumptions. In particular, complex secondary flow phenomena in the viscous flow field cannot be considered wherefore a final validation of the design by Computational Fluid Dynamics (CFD) is always required. Standard CFD-methods can also be coupled with optimization algorithms to identify designs of maximum efficiency. Numerous recent examples of CFD-based optimization exist, see e.g. the book by Thévenin and Janiga [3] from 2008. While this methodology is much more precise as compared to BEM or inverse design it suffers from the long computational time to obtain CFD solutions. To overcome this bottleneck, many recent studies tried to replace CFD by CFD-trained meta-models (e.g. response surface or artificial neural network, ANN). The idea behind this approach is to use CFD only to obtain a database for the training of meta-models, but to use the much quicker meta-models for the function evaluations in the optimization algorithms. The commercial application of this design process is e.g. offered by Numeca and several recent conference contributions describe successful design projects [4-6]. Similar projects are done by Aero Designworks, see conference contributions [7-9]. Although the development process can be shortened significantly due to the utilization of ANNs, there is still

much effort required for generating the CFD database. Moreover, all these publications only report a specific design project where the time-consuming CFD simulations need to be repeated for each new project due to a different design target and/or additional constraints.

In 2014, the authors of this work already presented ANNs with a geometrical input space that takes into account design points in the complete realm of axial or mixed-flow fans according to Cordier's diagram [10]. With these ANNs, renewed CFD simulations due to changes in design target are not any longer necessary. In the present work, these ANNs are applied to derive general rules for the choice of optimal geometrical parameters in the complete realm of low pressure axial fans. Here, "optimal" means designs with a maximum total-to-static efficiency

$$\eta_{ts} = \frac{\dot{V} \Delta p_{ts}}{P_{shaft}} \quad (1)$$

with the total-to-static pressure rise  $\Delta p_{ts} = p_2 - p_{t,1}$  which is static pressure downstream of the fan ("2" for downstream) minus total pressure upstream of the fan ("1" for upstream, "t" for total).

For the sake of comparability and transferability, it is adequate to introduce dimensionless coefficients for flow rate and pressure rise which will be used throughout this paper. As usual in turbomachinery, flow rate and pressure rise are non-dimensionalized with the fan diameter ( $D$ ), rotational speed ( $n$ ) and fluid density ( $\rho$ ):

$$\phi = \frac{\dot{V}}{\frac{\pi^2}{4} D^3 n}, \quad \psi = \frac{\Delta p}{\frac{\pi^2}{2} D^2 n^2 \rho} \quad (2, 3)$$

## METHODOLOGY

### Parameter Space

The geometrical parameters chosen for variation during optimization are more or less the classical, see e.g. Carolus and Starzmann [11]. The idea behind is to ensure a similar diversity of potential fan geometries as by state-of-the art design tools. Basic geometrical parameters are the hub-to-tip ratio ( $\nu$ ) and the number of blades ( $z$ ). The stagger angle ( $\gamma$ ) is set up in two steps. Firstly, a fictitious flow coefficient is estimated ( $\phi_{est}$ ) and used to compute the angle at which the incoming flow impinges on the rotating blade. This angle ( $\beta$ ) varies along the radius ( $r$ ) due to increasing circumferential velocity towards the blade tip and can be computed as

$$\beta(r) = \tan^{-1} \left( \frac{D}{2 \cdot r} \cdot \frac{\phi_{est}}{1 - \nu^2} \right). \quad (4)$$

Secondly, the blade stagger angle is computed as the sum of  $\beta$  and the local incidence angle  $\alpha$ :

$$\gamma(r) = \beta(r) + \alpha(r) \quad (5)$$

$\alpha$  is specified at five equidistant radial stations between hub and tip and a fourth degree polynomial is used for interpolation.  $\alpha$  can be distributed along the blade span for implementation of local effects, e.g. varying the spanwise load distribution.

A blade section is described by its chord length ( $c$ ), sweep angle ( $\lambda$ ), maximum camber/thickness ( $f$ ,  $d$ ) and position of maximum camber/thickness ( $x_f$ ,  $x_d$ ) of the utilized four digit NACA sections. The

reason for the choice of these classical NACA sections is the high level of geometrical flexibility provided by only few parameters. Each of the parameters describing the sections is defined at hub, mid-span, and tip with second degree polynomial interpolation in between. The sweep angle ( $\lambda$ ) is defined as the angle between the incoming relative velocity  $w_1(r, \phi_{est}, v)$  and the blade stacking line which goes through the center of gravity of each section. Details about the blade construction incorporating a sweep angle as well as its aerodynamic and acoustic effect are given by Beiler and Carolus (1999) [12].

The tip clearance ratio  $S/D$  is kept constant as it is pointless to optimize this parameter. It should always be as small as possible within the practical limitations regarding operating safety. As we consider aerodynamically optimized fans in this work, a rather small value (0.1 %) is selected. Fan diameter, fan speed, and air density are constant and amount to  $D = 0.3$  m,  $n = 3000$  min<sup>-1</sup>, and  $\rho = 1.185$  kg/m<sup>3</sup>. Strictly speaking, this limits the validity of our findings to the resulting Reynolds number ( $Re \approx 200,000$ ). However, the effect of varying Reynolds number can be estimated by the method suggested by Pelz and Stonjek in 2013 [13]. Most geometrical parameters are illustrated in Figure 2. Tab. 1 gives an overview about the range in which the parameters were varied.

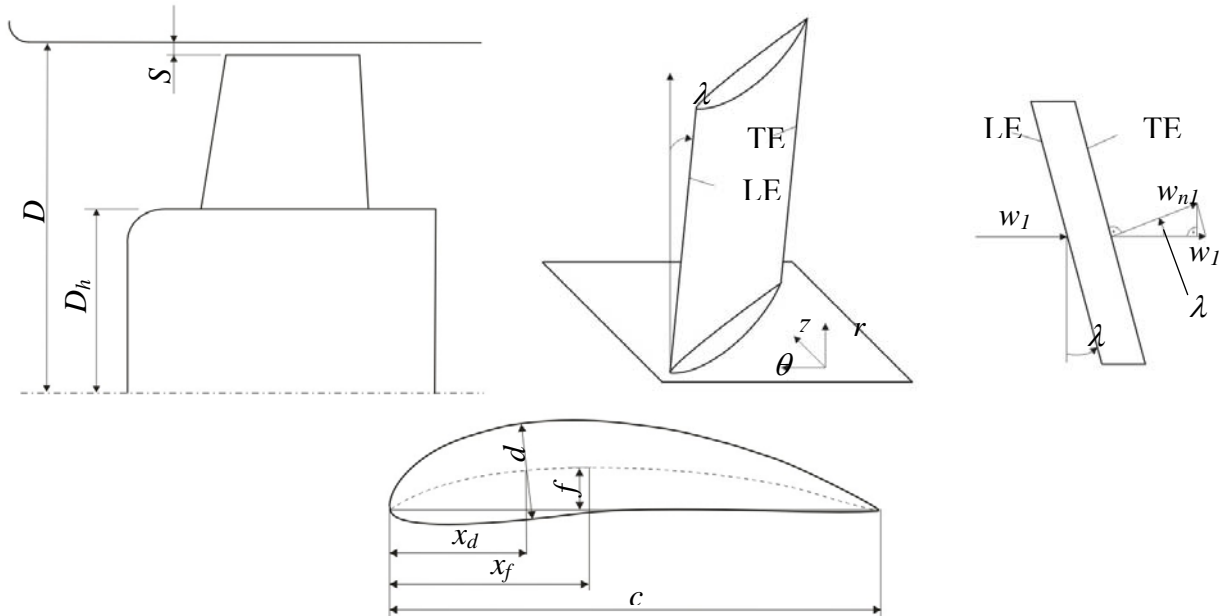


**Figure 2: Illustration of geometrical input parameters. Top left: Side view of a fan in a duct. Top right: Definition of the blade sweep angle in a 3D and 2D view (here: constant sweep angle from hub to tip). Bottom: Blade section**

### Meta-Model Training

As mentioned in the introduction, the meta-models used here are based on a previous work by the authors in 2014. For that reason, the following description of the training strategy is kept very short. All details can be found in reference [10].

The geometrical parameters were varied by a space-filling Design of Experiment (DoE). Each alternative fan design corresponds to one set of geometrical parameters. The performance data of each fan was computed by a steady-state Reynolds-averaged Navier-Stokes method (RANS). For that, the rotating computational domain was discretized with the commercial grid generator ANSYS TurboGrid® 14.5. All grids are block-structured and contain approx. 500,000 hexahedral elements. The computational domain covers a region of one fan diameter upstream and two fan diameters downstream of the fan blade. A general grid interface (GGI) was placed in the tip clearance. To save computational time, only one blade passage, with periodic boundary conditions at both sides, was simulated. Further boundary conditions were rotational speed, given mass flow rate at the inlet,

ambient pressure at the outlet and no slip at the walls (hub, shroud, and blade). Due to the rather small tip Mach number ( $Ma_{tip} = 0.14$ ) incompressible flow was assumed. The selected turbulence model was shear stress transport (SST). The RANS equations were solved with ANSYS CFX 14.5. The fan performance curves were evaluated between the two points the operating points of maximum total-to-static efficiency,  $\phi(\eta_{ts,max})$ , and zero total-to-static pressure coefficient,  $\phi(\psi_{ts}=0)$ . The resolution of  $\phi$  between these bounds was  $\Delta\phi = 0.02$ . This procedure of generation of geometry, meshing, simulation, and post-processing was automated, leading to a constantly increasing database. Characteristics based on non-converged CFD solutions were sorted out in order to avoid too much noise in the meta-model training data. Convergence is assessed by the maximal residuals with respect to conservation of mass and momentum ( $<10^{-3}$ ) as well as by the fluctuations of integral target values (e.g.  $\psi$ ,  $\eta$ ) over the last 20 iterations ( $<1\%$ ). As the exclusion of simulations leads to an unbalanced filling of the input space, the space-filling DoE is repeated from time to time taking the distribution of existing points into account. The grid independence was proven by simulating aerodynamically optimized fans with considerably finer grids containing up to 5,700,000 nodes. It was found that the discretization error with respect to  $\psi_{ts}$  and  $\eta_{ts}$  is less than 1%.

The final CFD database contains around 13,000 fan curves and was used to train ANNs of the multilayer perceptron (MLP) type. The MLPs consist of the input layer, two hidden layers with sigmoid neurons and one output layer with linear neurons. Optimization of the hidden layer weights was done by the Levenberg-Marquandt algorithm [14]. Network structure optimization (the number of neurons in each hidden layer) was done by an in-house algorithm based on the principle ideas of the steepest descent method. From the numerous MLPs that were constructed, only the ones that predict  $\psi_{ts}$  and  $\eta_{ts}$  will be used in the present work.

**Table 1: Definition and ranges of the 26 varied geometrical parameters**

Name	Symbol/Definition	Range	Remark
Estimated flow coefficient	$\phi_{est}$	0.05 – 0.7	Required for $\gamma$ and $\lambda$
Number of blades	$z$	5 – 11	Only integers
Hub-to-tip ratio	$\nu = D_h / D$	0.3 – 0.7	
Incidence angle <sup>2</sup>	$\alpha_h, \alpha_{0.25}, \alpha_m, \alpha_{0.75}, \alpha_t$	0° – 15°	Against $w_I$ vector
Chord length ratio <sup>1</sup>	$c_h/D_h, c_m/D_m, c_t/D_t$	0.133 – 0.333	
Rel. max. camber <sup>1</sup>	$f_h/c_h, f_m/c_m, f_t/c_t$	0 – 0.15	NACA section
Rel. position of max. camber <sup>1</sup>	$x_{f,h}/c_h, x_{f,m}/c_m, x_{f,t}/c_t$	0.1 – 0.7	NACA section
Rel. max. thickness <sup>1</sup>	$d_h/c_h, d_m/c_m, d_t/c_t$	0.05 – 0.12	NACA section
Rel. position of max. thickness <sup>1</sup>	$x_{d,h}/c_h, x_{d,m}/c_m, x_{d,t}/c_t$	0.1 – 0.5	NACA section
Sweep angle <sup>1</sup>	$\lambda_h, \lambda_m, \lambda_t$	-60° - +60°	Against $w_I$ vector

<sup>1</sup> At three equidistant radial positions with polynomial interpolation in between

<sup>2</sup> At five equidistant radial positions with polynomial interpolation in between

### Generation of Rules for Optimal Geometrical Parameters

The energetically optimal choice of each parameter ( $y$ ) shall be determined by a two-dimensional second degree polynomial with the two inputs  $\phi$  and  $\psi_{ts}$ :

$$y = \sum_{i=0}^2 \sum_{j=0}^2 a_{ij} \phi^i \psi_{ts}^{j-i} \quad (6)$$

According to Eq. 6 there are six polynomial coefficients  $a_{ij}$  per parameter; hence the optimization problem consists in finding the  $6 \times 26 = 156$  coefficients that lead to maximal  $\eta_{ts}$  for targeted design points ( $\phi$ ,  $\psi_{ts}$ ). Finding optimal coefficients is conducted in two steps. In the first step, the targeted design point is varied systematically and the 26 geometrical parameters are optimized for each point. The polynomials are then determined as best-fit curves through the thus obtained optimal

parameters. In the second step, the polynomial coefficients are directly optimized using the result of step one as the initial solution. Subsequently, the two steps will be explained in more detail.

Step 1: Optimization of Geometrical Parameters

$\phi$  is varied between 0.08 and 0.24 with a step size of 0.02. Analogously,  $\psi_{ts}$  is varied between 0.06 and 0.38 with a step size of 0.04. For each of the resulting 81 combinations, the 26 geometrical parameters are optimized by an evolutionary optimization algorithm. The first generation is obtained by DoE and the reproduction of subsequent generations is based on the cross-over method, i.e. mixing of genes (the parameter values) of the previous generation. The probability of a parent individual to participate in the reproduction process is based on its target function value. Here, the target function is maximization of  $\eta_{ts}$  considering a penalty term for violation of the targeted design point by the MLP-prediction:

$$\eta^* = \eta_{ts,MLP-predicted} - k \left| \psi_{ts,MLP-predicted} - \psi_{ts} \right| \quad (7)$$

The factor  $k$  weights the significance of the penalty term and is here set to five. Since the function evaluation by means of the MLPs is extremely quick, it is affordable to use a huge number of generations and a huge number of individuals per generations (10,000 each) to ensure that the global optimum is found.

As a result of the optimization, the optimal geometrical parameters of each of the 81 design points are known and curve-fitting can be conducted to approach the dependency between targeted design point and optimal geometrical parameters values by polynomials. The curve-fitting to find the polynomial coefficients is basically a simple least-squares problem. However, the problem is extended by a special treatment of parameter values which converged to the lower or upper bound according to Tab. 1. In that case, it is acceptable if the polynomial suggests parameter values below or above the bounds, respectively. This is not problematic as such values can be repressed to the bounds manually. The reason for that approach is to enable a better fit for the values within the bounds.

Step 2: Optimization of the Polynomial Coefficients

The result of step one represents a good starting point but is not yet satisfactory because the optimization procedure did not consider that all optimal parameter values must fit on a second degree polynomial later on. This can be improved by considering all design points simultaneously in one target function. The parameters to be optimized then no longer are the geometrical parameters of one fan but the polynomial coefficients which are the basis of all fans. The target function becomes

$$\eta^* = \sum_{i=1}^{81} \left( \eta_{ts,MLP-predicted,i} - k \left| \psi_{ts,MLP-predicted,i} - \psi_{ts,i} \right| \right)^2 \quad (8)$$

where  $i = 1 \dots 81$  represents the 81 distinct design points.

The 156 coefficients are optimized by an evolutionary algorithm. The first generation consists of the solution from step one with moderate random mutations. The reproduction of a subsequent generation is again based on the cross-over method. However, a gene now consists of the six coefficients which describe the polynomial of one geometrical parameter. The reason for not separating the coefficients of the same geometrical parameter is to maintain a reasonable shape of the polynomials. New shapes can develop by random mutation of the coefficients which is applied at the end of each reproduction process.

# RESULTS

## Optimal Geometrical Parameters as a Function of Design Point

Figure 3 depicts charts that can be used to determine the optimal geometrical parameters as a function of  $\phi$  and  $\psi_{ts}$ . The following discussion of the charts is more a description with only basic consideration of the aerodynamic background. A more profound analysis of the aerodynamic background is conducted in further publication [15].

The most relevant geometrical parameters are  $\phi_{est}$ ,  $z$ , and  $\nu$  (subplot 1-3). The qualitative shape of their curves was expected.  $\phi_{est}$  increases with  $\phi$  which simply means that the stagger angle needs to be adjusted to the flow angles.  $\phi_{est}$  also increases with  $\psi_{ts}$  which results from the necessity to deflect the flow sufficiently to realize big values of  $\psi_{ts}$ . Moreover, the effective flow angle (obtained from the vector-mean of the relative velocities upstream and downstream of the fan) grows with increasing flow deflection which also contributes to higher values of  $\phi_{est}$ .

The graphs for the number of blades show a similar behavior. Increasing pressure coefficient leads to the need for higher solidity which can e.g. be achieved by more blades. Note that the graphs shown are continuous and that the number of blades needs to be rounded to integers for real-life applications.

The hub-to-tip ratio can be used to control the throughflow velocity by reducing the cross-section area at small flow rates and increasing it at large flow rates. The hub size also increases with increasing pressure rise which is typical for axial fans and qualitatively meets the findings by Eck in 2003 [16]. A quantitative comparison is conducted later in the paper.

Further geometrical parameters which have a definite effect on the load are the chord length  $c$  (subplot 4-5) and the camber  $f$  (subplot 10-12). Again, both parameters rise with increasing  $\psi_{ts}$ . On top of that, they rise with increasing  $\phi$  to compensate increasing exit losses. The only exception is the chord length at the hub which is always as large as possible. This and other parameters which always converged to the upper or lower bound of the parameter space irrespectively of the design point are listed in Tab. 2.

An interesting relation is found for the local incidence angle  $\alpha$  depicted in the subplots 6-9. For most design points, the greatest values occur at 25% blade height from where the angle decreases continuously until 75% blade height. However, untypical relations are found for the endplate regions (hub and tip). The hub region is unloaded as much as possible ( $\alpha_h = 0^\circ$ ), see Tab. 2. Towards the tip, the targeted pressure coefficient plays a much more significant role as compared to other blade regions. Therefore, the aforementioned tendency for decreasing incidence angles along the blade height can be reversed close to the tip in case of high targeted pressure coefficients.

The design guidelines for the section details ( $x_f/c$ ,  $d/c$ ,  $x_d/c$ ) are depicted in the subplots 13-16. Many of those parameters converged to the bounds of the parameter space and are consequently listed in Tab. 2.

The optimal sweep angle rises with flow rate (subplot 17-19). At hub and tip, high targeted pressure coefficients lead to small sweep angles while the opposite is observed at midspan. The intensity of these dependencies varies along the span and is weakest at midspan which leads to only moderate sweep angles between  $-20^\circ \leq \lambda_m \leq +20^\circ$ . However, stronger sweep is often required for acoustic reasons or for the extension of operating range. If stronger sweep is enforced, the peak efficiency of moderately swept blades can be restored by adjusting other geometrical parameters to the enforced sweep angles. However, the extent of the required adjustments cannot be estimated by design charts but has to be determined by individual optimization projects.

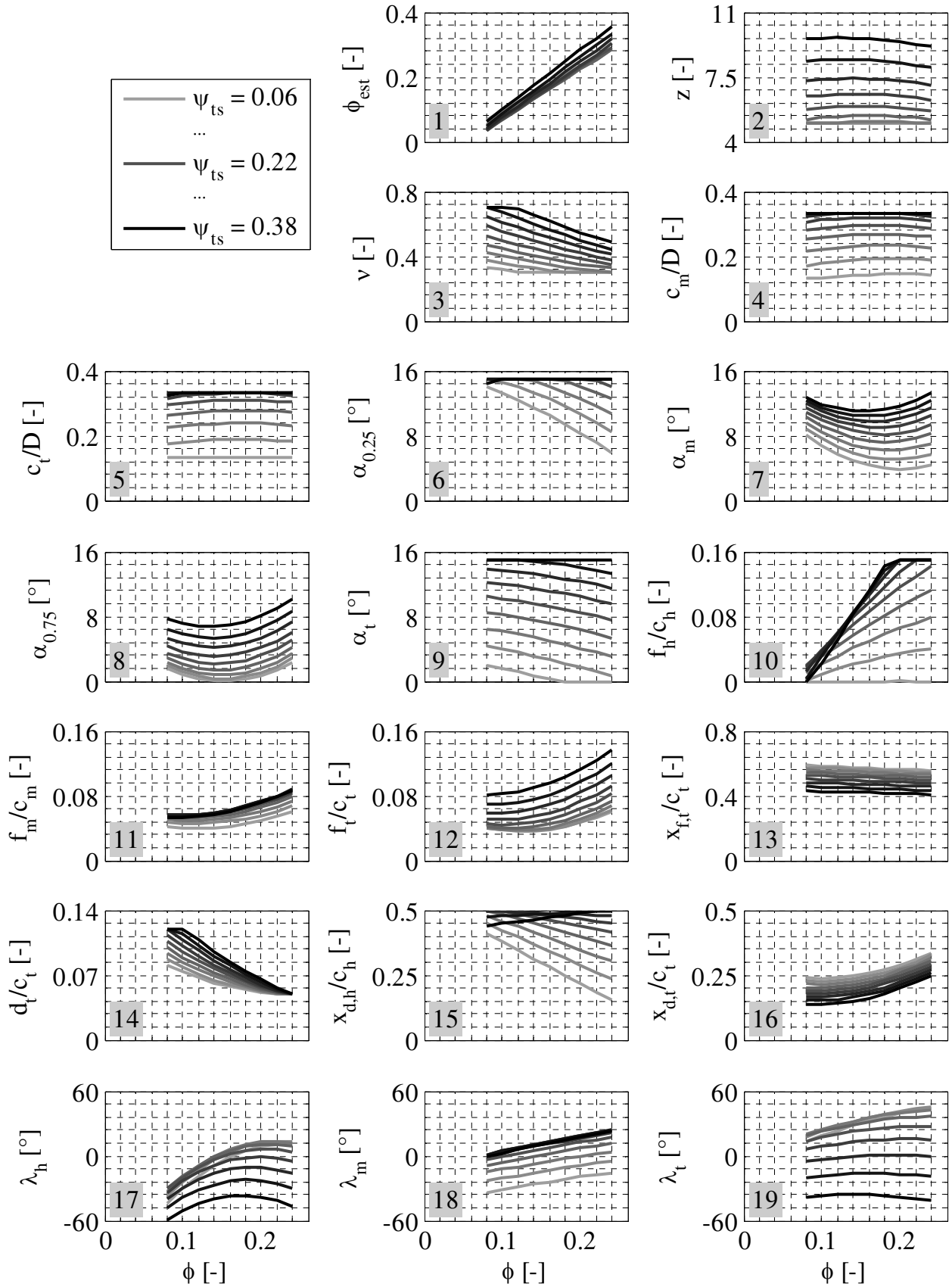


**Figure 3: Optimal parameters as a function of flow and pressure coefficient. The indices  $h$ ,  $m$ , and  $t$  represent the hub, midspan, and tip section of the blade, respectively. In case of  $\alpha$ , the additional indices 0.25 and 0.75 correspond to 25 or 75 % blade height, respectively.**



**Table 2: Parameters of which the optimal value is independent from the design point**

Name	Symbol	Optimal value	Remark
Chord length at hub	$c / D$	0.333	upper bound of range
Incidence angle at hub	$\alpha_h$	0°	lower bound of range
Position of max. camber at hub	$x_{f,h} / c_h$	0.7	upper bound of range
Position of max. camber at midspan	$x_{f,m} / c_m$	0.2	lower bound of range
Max. thickness at hub	$d_h / c_h$	0.12	upper bound of range
Max. thickness at midspan	$d_m / c_m$	0.05	lower bound of range
Position of max. thickness at midspan	$x_{d,m} / c_h$	0.1	lower bound of range

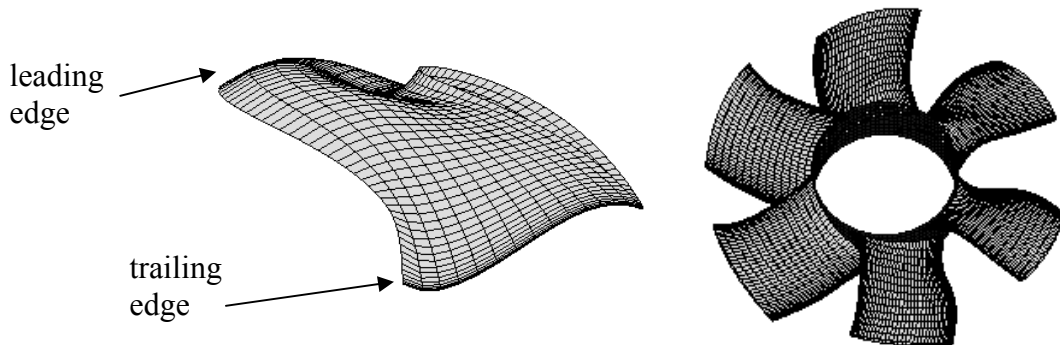
### Application and Validation of the Rules for Choosing Optimal Geometrical Parameters

An example of how to determine the optimal parameter values will be given for the design point  $\psi_{ts} = 0.22$  at  $\phi = 0.18$ . Basically, all geometrical parameters which determine the blade shape can be read from Figure 3 or from Tab. 2. Only the stagger  $\gamma$  requires an additional step as it is always a result of the interaction between  $\phi_{est}$ ,  $\nu$ , and  $\alpha$ .  $\phi_{est}$  and  $\nu$  determine the estimated inflow angle  $\beta_{est}$  (Eq. 4) which is added to  $\alpha$  to obtain  $\gamma$ . The thus obtained optimal parameters for the current example are listed in Tab. 3. Figure 4 shows the resulting fan in a 3D view. 15 radial cuts were used for that Figure. As mentioned before, an arbitrary number of radial cuts can be considered by polynomial interpolation between the positions at which the geometrical parameters are defined.

**Table 3: Optimal Geometrical Parameters for the Sample Design Point  $\psi_{ts} = 0.22$  at  $\phi = 0.18$** 

Parameter	Optimal value(s) <sup>1</sup>	Remark
$\phi_{est}$	0.199	With these values for $\phi_{est}$ and $\nu$ , Eq. 4 yields $\beta = [28.1 \ 21.3 \ 17.0 \ 14.2 \ 12.2]^\circ$
$\nu$	0.402	
$\alpha$	$[0 \ 15 \ 7.5 \ 2.6 \ 8.9]^\circ$	Eq. 5 yields the resulting stagger angle $\gamma = \beta + \alpha = [28.1 \ 36.3 \ 24.6 \ 16.8 \ 21.0]^\circ$
$z$	5.89	rounded to 6 for real-life application
$c/D$	$[0.33 \ 0.30 \ 0.31]$	
$f/c$	$[0.099 \ 0.064 \ 0.053]$	
$x_f/c$	$[0.70 \ 0.20 \ 0.70]$	
$d/c$	$[0.120 \ 0.050 \ 0.061]$	
$x_d/c$	$[0.50 \ 0.10 \ 0.10]$	
$\lambda$	$[7.0 \ 10.2 \ 23.2]^\circ$	in the direction of $w_1$

<sup>1</sup> If more than one value is given, the values refer to equidistant positions between hub and tip. Polynomials shall be used to obtain a continuous distribution along the span.

**Figure 4: 3D view of a blade and a fan designed with optimal geometrical parameters for the**

### design point $\psi_{ts} = 0.22$ at $\phi = 0.18$

The procedure described above is conducted for all of the aforementioned 81 design points and the resulting fans are simulated by means of RANS. Figure 5 shows the difference between the targeted design points and the CFD results. Good agreement can be achieved for almost all design points. The maximum deviation amounts to  $\Delta\psi_{ts} = \psi_{ts} - \psi_{ts,CFD-predicted} \approx 0.02$ .

The right side of Figure 5 shows the achievable efficiency which strongly depends on the design point. Design points with high flow rate or high pressure rise suffer from high exit losses due to the through-flow velocity or swirl velocity, respectively. However, if  $\psi_{ts}$  becomes too small, there is also a decay of  $\eta_{ts}$  because the static share of the total-to-total pressure rise becomes too small. The peak efficiency is limited by  $\eta_{ts} < 0.68$  which agrees with the findings of the earlier investigations in 2014 [10].

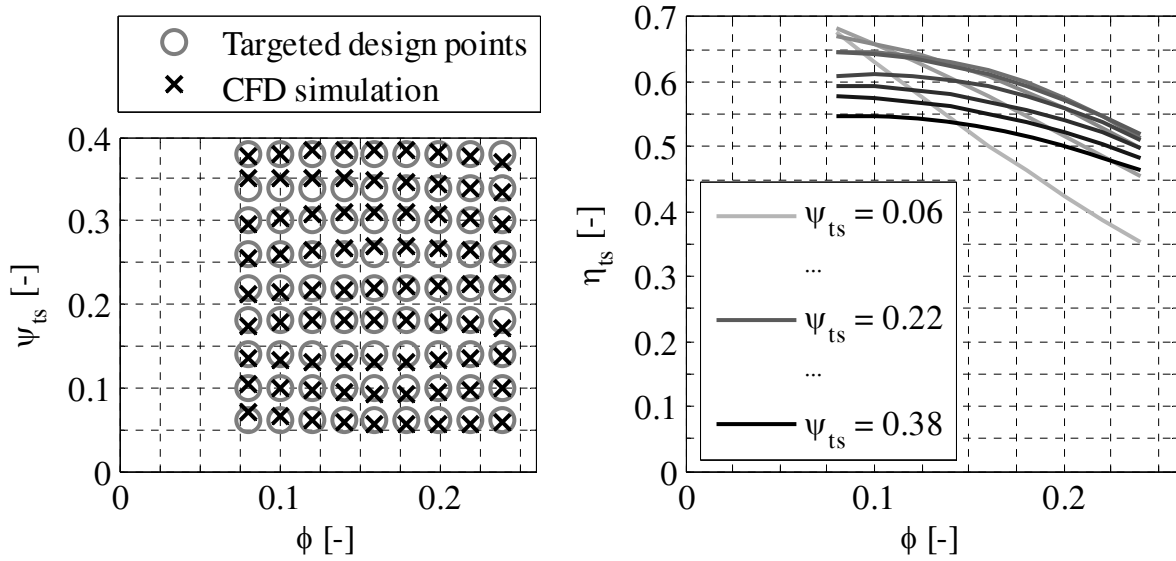


**Figure 5: CFD-assessment of fans designed with optimal geometrical parameters. Left: comparison between targeted design point and CFD prediction. Right: achievable total-to-static efficiency according to CFD.**

### Comparison with Existing Design Recommendations

One essential parameter for the maximization of  $\eta_{ts}$  is the hub-to-tip ratio ( $\nu$ ). Guidelines for the choice of  $\nu$  have been provided by Eck in 2003 [16]. While the recommendations by Eck show the same trends regarding dependency on flow rate and pressure rise, the magnitude of  $\nu$  is much smaller in the present study, see Figure 6. Since Eck presents  $\nu$  as a function of specific fan speed ( $\sigma$ ) and specific fan diameter ( $\delta$ ) it was necessary to compute these values for each of the present design points. For that, the total-to-total pressure coefficient ( $\psi_{tt}$ ) is required which was determined by another MLP from the work in reference [10].

There are two main reasons for the massive reduction of hub size as compared with Eck's recommendation. On the one hand, the focus of this work is the optimization of  $\eta_{ts}$  which always requires small hubs to reduce exit losses whereas there is no hint that  $\eta_{ts}$  was also the main target of Eck. On the other hand, such small hubs are only feasible if the fans are carefully optimized and all other parameters are adjusted to the small hub size to avoid flow separation and additional secondary flows. This optimization is done in the present work whereas Eck's work is based on investigations of standard designs.

Other contemporary design recommendations deal with the resulting flow field instead of with the geometrical parameters themselves. Carolus [1] cites three validity limits with should be considered to avoid extensive secondary flows and losses. The criterion by de Haller demands that

the deceleration of the flow is limited by  $w_2/w_1 \geq 0.55$ . The criterion by Strscheletzky demands sufficient throughflow velocity relative to the swirl velocity, i.e.  $c_{m2}/c_{\theta 2} \geq 0.8$ . The criterion by Lieblein deals with the diffusion number ( $DF$ ), defined as

$$DF = \left(1 - \frac{w_2}{w_1}\right) + \left(\frac{1}{2\sigma} \frac{\Delta w_\theta}{w_1} + \frac{d}{c}\right) \quad (9)$$

where  $\sigma$  is the solidity and  $w_\theta$  is the relative velocity in circumferential direction. The upper limit of  $DF$  is given by 0.8. It is found that from the 81 optimal designs investigated in this study only 32% comply with de Haller, 6% comply with Strscheletzky and 48% comply with Lieblein. Hence, optimization appears to be a suitable tool to overcome these criteria provided that the RANS model used here is accurate enough. However, it must be acknowledged that the present study only focuses on the design point. Fans designed in accordance with the validity criteria usually have a reasonable distance between the design point and the stall point. Whether or not this margin also exists for fans designed according the guidelines has not yet been investigated.

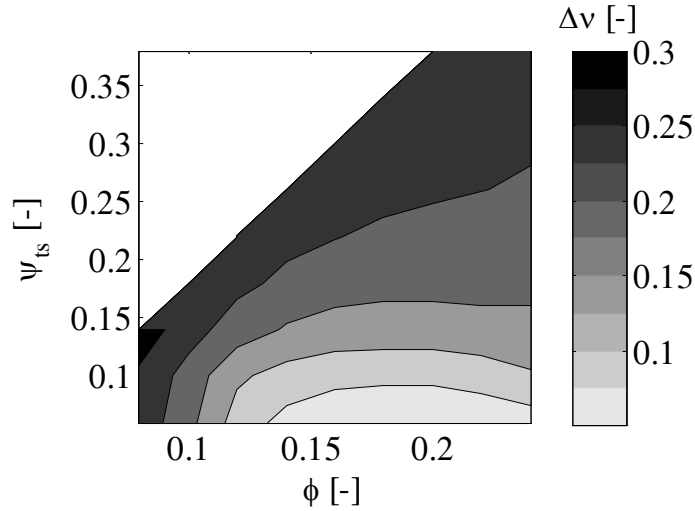


**Figure 6: Difference between the hub-to-tip ratio recommended by Eck [16] and the hub-to-tip ratio according to the findings of this work. No data by Eck exists for the top left corner**

## CONCLUSIONS

Design guidelines for the optimal choice of 26 geometrical parameters of low pressure axial fans are suggested. "Optimal" here means fulfilment of a targeted design point at maximum possible total-to-static efficiency. This design strategy is a good alternative for analytical design tools which are imprecise due to many simplifying assumptions or CFD-optimization which is time-consuming and requires large computational recourses. From all geometrical parameters, the hub-to-tip ratio was discussed in most detail. Since the guidelines are developed for maximal possible total-to-static efficiency, the recommended hub-to-tip ratios become much smaller as compared to previous studies, e.g. by Eck [16].

81 fans with distinct design points between  $0.08 \leq \phi \leq 0.24$  and  $0.06 \leq \psi_{ts} \leq 0.38$  were designed according to the guidelines and simulated by the RANS method. The CFD results confirm the validity of the guidelines as the targeted design points were met with good agreement and a high level of total-to-static efficiency was achieved.

Ongoing work focuses on two main fields of research. On the one hand, it is tried to find more profound aerodynamic explanations for the outcomes of this work. For that, three characteristic design points are selected at which fans designed according to the guidelines will be compared with state-of-the art fans in more detail. The second field of research deals with dependencies between

the geometrical parameters. In practical applications there might be constraints with respect to some of the geometrical parameters, e.g. a strong blade sweep can be enforced for acoustic reasons. In such cases it is important to know if the other geometrical parameters can still be determined according to the guidelines presented here or if the change of one geometrical parameter also affects the optimal choice of others. In particular, it is interesting to find out which other geometrical parameters are essential to enable the small hub sizes recommended in this work.

## REFERENCES

1. Carolus, T., *Ventilatoren - Aerodynamischer Entwurf, Schallvorhersage, Konstruktion*. Vol. 3. Auflage. 2012, Wiesbaden: Springer Vieweg.
2. Zangeneh, M., *A Compressible Three-Dimensional Design Method for Radial and Mixed Flow Turbomachinery Blades*. International Journal of Numerical Methods in Fluids, 1991. **13**(5): p. 599-624.
3. Thévenin, D. and G. Janiga, *Optimization and Computational Fluid Dynamics*. 2008, Heidelberg: Springer Verlag GmbH.
4. Demeulenaere, A., et al. *Design and optimization of an industrial pump: Application of genetic algorithms and neural networks*. in *ASME Fluids Engineering Division Summer Meeting & Exhibition*. 2005. Houston, TX.
5. Pierret, S. and C. Hirsch, *An Integrated Optimization System for Turbomachinery Blade Shape Design*. 2003: Defense Technical Information Center.
6. Hildebrandt, T., A. Starke, and G. Ruck. *Leistung- und Effizienzsteigerung einer Diagonallüfterstufe: Von der CFD basierten Optimierung mit FINE™/Turbo bis zur Serieneinführung*. in *VDI Ventilatoren*. 2010.
7. Siller, U., C. Voß, and E. Nicke. *Automated Multidisciplinary Optimization of a Transonic Axial Compressor*. in *47th AIAA Aerospace Sciences Meeting*. 2009. Florida: American Institute of Aeronautics and Astronautics.
8. Siller, U. and C. Voß. *Multidisciplinary 3D-Optimization of a Fan Stage Performance Map with Consideration of the Static and Dynamic Blade Mechanics*. in *ASME TurboExpo*. 2010. Glasgow, UK.
9. Kröger, G., R. Schnell, and N. Humphreys. *Optimised Aerodynamic Design of an OGV with Reduced Blade Count for Low Noise Aircraft Engines*. in *ASME TurboExpo*. 2012. Copenhagen, Denmark.
10. Bamberger, K. and T. Carolus. *Performance Prediction of Axial Fans by CFD-Trained Meta-Models*. in *ASME TurboExpo 2014*. 2014. Düsseldorf, Germany.
11. Carolus, T. and R. Starzmann. *An Aerodynamic Design Methodology for Low Pressure Axial Fans with integrated Airfoil Polar Prediction*. in *ASME TurboExpo 2011*. 2011. Vancouver, Canada.
12. Beiler, M. and T. Carolus, *Computation and Measurement of the Flow in Axial Flow Fans With Skewed Blades*. Journal of Turbomachinery, 1999. **121**: p. 59-66.
13. Pelz, P. and S. Stonjek, *The Influence of Reynolds Number and Roughness on the Efficiency of Axial and Centrifugal Fans—A Physically Based Scaling Method*. Journal of Engineering for Gas Turbines and Power, 2013. **135**(5).
14. Marquardt, *An Algorithm for Least-Squares Estimation of Nonlinear Parameters*. SIAM Journal of Applied Mathematics, 1963. **11**: p. 431-441.
15. Bamberger, K. and T. Carolus. *Analysis of the Flow Field in Optimized Axial Fans*. in *ASME TurboExpo*. 2015. Montreal, Canada.
16. Eck, B., *Ventilatoren*. Vol. 6. Auflage. 2003: Springer Verlag.